Pergamon

*Journal of Structural Geology*, Vol. 17, No. 8, pp. 1183 to 1195, 1995

0191-8141/95 $9.50+0.00

0191-8141(95)00004-6

# The rise of solid-state diapirs

ROBERTO F. WEINBERG*

Hans Ramberg Tectonic Laboratory, Institute of Earth Sciences, Uppsala University, Norbyvägen 18B, S-752 36 Uppsala, Sweden

and

YURI YU. PODLADCHIKOV†

Institute of Earth Sciences, Vrije Universiteit, De Boelelaan 1085, 1081 HV, Amsterdam, The Netherlands

(*Received* 16 *May* 1994; *accepted in revised form* 19 *December* 1994)

**Abstract**—When magma inside a diapir solidifies it increases in density and becomes a stiff power-law fluid. If the diapir is still positively (or negatively) buoyant after solidification, it will continue to rise (or start to sink). The results presented here suggest that solidified diapirs may rise (sink) a distance of up to a few kilometres in geologically reasonable times. Rocks and bubble- and/or crystal-rich magmas behave as power-law fluids. This paper compares numerical results of viscosity and strain-rate profiles across power-law and Newtonian diapirs and wall rocks. The comparison shows that the core of power-law diapirs deforms more slowly and the margins much faster than in Newtonian diapirs. This pattern of strain rate distribution leads to the often observed isotropic or weakly deformed core surrounded by a strongly sheared margin. Furthermore, the results suggest that the strain rate of the ambient fluid (wall rock) is imposed across the contact into a power-law diapir resulting in similar strains on either side of the contact, and that power-law wall rocks, in contrast to Newtonian wall rocks, deform into a rim synform as the diapir rises.

## INTRODUCTION

The rise of magma diapirs is often implicitly assumed in the geological literature to end with the completion of crystallization, because of increased diapir viscosity or loss of buoyancy. This paper argues that this need not be the case, and that the solid-state diapir will continue to ascend if the body remains buoyant. Conversely, if the diapir becomes negatively buoyant during solidification it may sink towards its neutral buoyancy level (Arndt & Goldstein 1989, Glazner 1994). Here we will concentrate on the continued rise of the diapir, but the results presented are equally applicable to sinking diapirs.

Several reported plutons are lighter than their wall rocks (e.g. Vigneresse 1988, Cruden & Aaro 1992, England 1992) indicating that they never attained a level of neutral buoyancy. A solid-state diapir will rise at velocities controlled by its buoyancy and the effective viscosity, dependent on the flow-law parameters, of both the diapir and the wall rock. Laboratory experiments have determined these parameters and shown that rock creep is likely to be power law with exponent $n$ of between 2.5 and 5 (Kirby 1983, Paterson 1987, Wilks & Carter 1990). Experimental and theoretical works on the rise of diapirs through the crust have considered the rise of either Newtonian or rigid spheres, through either Newtonian (e.g. Marsh 1982, Cruden 1988, 1990, Schmeling *et al.* 1988, Weinberg 1992) or power-law fluids (e.g. Mahon *et al.* 1988, Miller *et al.* 1988, Weinberg & Podladchikov 1994). It is the aim of this paper to study both the velocity of rise and the pattern of viscosity and strain-rate distribution inside and around a power-law diapir. The results presented here enable a better understanding of a number of emplacement-related structures observed in nature, such as the superimposition of solid-state foliation on magmatic foliation, and increasing foliation intensity towards the diapir's contact, strain gradation across the contact, a narrow strain aureole and a rim synform.

## PREVIOUS WORK

Experiments suggest that creep in both rocks and magmas is strain-rate dependent. The rheology of magmas, however, depends in a complex way on several factors such as strain rate, composition, temperature, pressure, and crystal, bubble and water content. A number of experiments have shown that magmas may either behave as Newtonian fluids (such as basalt above its liquidus temperature, Shaw 1969) or as power-law or Bingham fluids (bubble- and/or crystal-rich magmas; e.g. Shaw 1969, Spera *et al.* 1988, Kerr & Lister 1991, Pinkerton & Stevenson 1992). Thus, the present study models the rise of both rocks and magmas.

The rise of magmatic diapirs may be geometrically represented by the rise of a spherical drop through

*Present address: Research School of Earth Sciences, Australian National University, Canberra, ACT 0200, Australia.

†Permanent address: Institute of Experimental Mineralogy, Russian Academy of Sciences, Chernogolovka, Moscow District, 142 432 Russia.

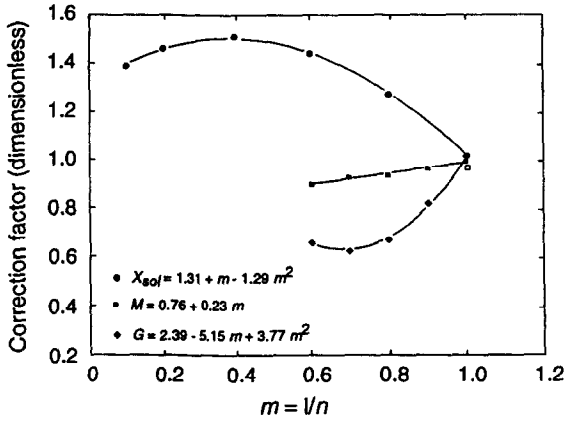


Fig. 1. Dimensionless correction factors for the extended Hadamard–Rybczynski equation (equation 1) as a function of $m = 1/n$. $X_{sol}$ from Crochet *et al.* (1984), and $G$ and $M$ obtained by the best fit of the data in Nakano & Tien (1968) by equation (1).

viscous fluids (e.g. Marsh 1982, Schmeling *et al.* 1988, Weinberg & Podladchikov 1994). Stokes' equation relates the velocity of a solid sphere sinking or rising through infinite Newtonian fluid to its buoyancy and the viscosity of the ambient fluid. Hadamard (1911) and Rybczynski (1911) extended Stokes' solution to Newtonian spheres and showed that the difference in velocity between a solid and an inviscid sphere in Newtonian fluids is only 1.5. In recent studies the present authors (Weinberg & Podladchikov 1993, 1994) extended the Hadamard–Rybczynski equation, with the help of three correction factors, to describe the rise of spherical or cylindrical viscous diapirs composed of Newtonian or power-law fluids, through power-law wall rocks

$$V = \frac{1}{3}\frac{\Delta\rho g r^2}{\eta_{\text{eff}}}\left(\frac{1}{X_{sol}}\frac{G\eta_{\text{eff}} + \eta_{\text{sph}}}{(GM\eta_{\text{eff}} + 1.5\eta_{\text{sph}})}\right)^n. \quad (1)$$

$\Delta\rho$ is the density difference between diapir and wall rock, $g$ the gravitational acceleration, $r$ the diapir's radius, $\eta_{\text{eff}}$ and $\eta_{\text{sph}}$ the effective viscosities of the ambient fluid and sphere respectively, and $X_{sol}$, $G$ and $M$ are dimensionless correction factors. These factors have values dependent only on the power-law exponent $n$ as depicted in Fig. 1 (from Weinberg & Podladchikov 1994). Using these correction factors, the velocity ratio between inviscid and solid spheres or cylinders can be shown to increase with the power-law exponent ($n$) of the wall rock and, for example, while for $n = 1$ this difference is 1.5, for $n = 5$ it is approximately 8.

The viscosity of a power-law fluid is not defined *a priori* but depends on the stress to which it is submitted. In the case of buoyant spheres and cylinders, the effective viscosity of the power-law wall rock, as well as that of the diapir itself, are a function of the buoyant stress of the diapir ($\Delta\rho gr$) according to (Weinberg & Podladchikov 1993, 1994)

$$\eta_{\text{eff}} = \frac{K^n 6^{n-1}}{(\Delta\rho g r)^{n-1}} \quad (2)$$

where $K^n$ depends on the rock flow-law parameters according to

$$K^n = \frac{1}{Ae^{-E/RT}3^{(n+1)/2}}. \quad (3)$$

$E$ is the activation energy in J mol$^{-1}$, and $A$ is the pre-exponential parameter in Pa$^{-n}$s$^{-1}$. When the effective viscosity ratio ($S$) between diapir and wall rock is small ($S = \eta_{\text{diapir}}/\eta_{\text{wall rock}} < 10^{-3}$) the crystalline diapir rises with the same velocity as an inviscid Newtonian diapir. Conversely, when $S > 10^3$ the velocity will be that of a solid Newtonian diapir. This is a natural result since for an effectively inviscid or solid diapir, the rheology of its fluid does not affect its rise.

The width of the strain aureole around plutons depends on how the space for the plume is created. Paterson & Fowler (1993) suggested that a combination of factors, such as viscous flow, rigid translation, stoping and assimilation of the wall rocks, as well as doming of the roof, controls the width of the strain aureole. Diapirs rising in purely viscous medium have an aureole width that decreases with increasing power-law exponent $n$ of the wall rock, consequently the flow concentrates towards the diapir (Weinberg 1994). The velocity profiles of the ambient fluid along the equatorial plane of a rising solid sphere (Fig. 2) show that for $n$-values above 1.7, the narrowing of the flow around the sphere causes a counterflow region close to the sphere where the fluid moves downwards faster than would be the case further from the diapir. The shape of these velocity curves controls the formation of rim synforms around diapirs.

## THE BRITTLE–DUCTILE TRANSITION AS A LIMIT TO DIAPIRISM?

The crustal depth at which the behaviour of rocks changes from ductile to brittle is often considered to be

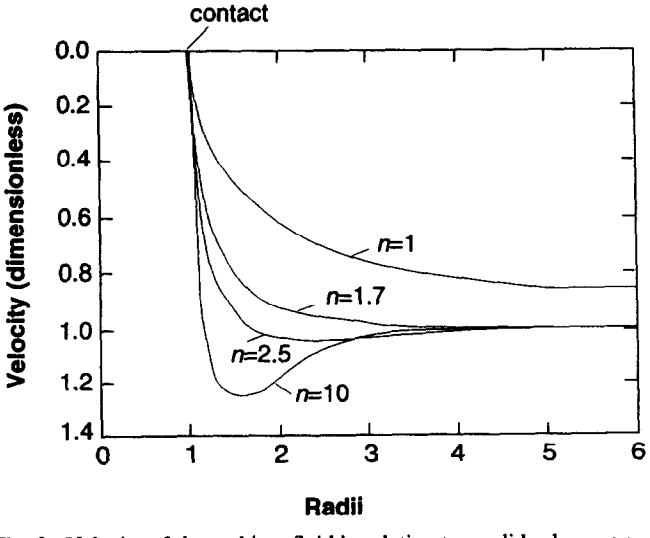


Fig. 2. Velocity of the ambient fluid in relation to a solid sphere as a function of distance from the sphere contact (redrawn from Crochet *et al.* 1984). The velocity is given as the difference between the velocity of the sphere and that observed, normalized by the difference between the velocity of the sphere and that at infinity. At the sphere's surface there is no slip and the fluid moves with the same velocity as the sphere. The overshooting of the velocity profiles observed for $n > 1.7$ indicates that the fluid moves down in relation to a fixed external marker, and faster than a fluid particle further away from the sphere.

an ultimate barrier for the rise of magmatic diapirs. A rising diapir is thought either to spread laterally under the brittle layer or to intrude it as dykes. The depth of the brittle–ductile transition is obtained from strength profiles of the crust where the Byerlee and power laws of rocks are plotted as a function of depth at constant strain rate; the b–d transition being the depth at which the differential stress is the same for both laws (see discussion in Carter & Tsenn 1987, Paterson 1987, Ord & Hobbs 1989). For common values of mountain-building strain rates, the b–d transition is usually between 10 and 20 km and depends on rock types, temperature profile (the geothermal gradient), the strain rate (or alternatively the size of differential stresses) and, according to Schmid & Handy (1991), on strain. The dependence of the b–d transition depth on the strain rate/stress and temperature is of special importance, since it implies dependence on whether the crust is under tension or compression (typically the b–d depth increases with increasing stress/strain rate).

Before discussing the relation between the b–d transition and diapirism, a brief discussion of the problem of nomenclature of deformation mechanisms is appropriate. Schmid & Handy (1991) suggest that the genetic terms 'frictional' and 'viscous' should be used rather than the often confusing terms 'brittle' and 'ductile'. As this genetic classification relates to two different types of rheological behaviour (rate-independent, pressure-sensitive frictional sliding and rate-dependent viscous flow), it perfectly suits our needs and the rationale concerning the depth of the b–d transition (or rather, using these new terms, the depth of frictional–viscous transition). Schmid & Handy discuss the ambiguity of the term 'ductile', which structural geologists and experimental rock mechanists use to describe the capacity of material to deform by uniformly distributed flow (for further references and discussion see Rutter 1986, Scholz 1990 p. 35, and Schmid & Handy 1991). In this paper we use the term 'ductile' as a synonym, in the genetic sense, to the term 'viscous' (caused by power-law creep), as is usual in the context of strength profiles of a deforming lithosphere.

A further ambiguity relates to the terms 'plasticity' and 'plastic deformation'. According to the mechanics of continuum media (e.g. Turcotte & Schubert 1982 p. 341, Mandl 1988), there are two distinct types of inelastic behaviour. The first is the rate-dependent creep below the yield strength, and the second is plastic yielding, usually rate independent. Thus, theoretically, brittle (frictional) behaviour is best described by an elasto-plastic (non-associated) rheological model (Mandl 1988), and the terms 'plasticity' and 'plastic irreversible deformation' apply to this type of behaviour. This is often the opposite of their meaning in structural geology and experimental rock mechanics where for example the terms 'superplasticity' and 'intracrystalline plasticity' are specific mechanisms of deformations that are rate controlled, and fall therefore into the 'viscous' type according to both Schmid & Handy and to classic mechanic classification. In view of these difficulties, we suggest either avoiding the use of the term 'plastic' in the context of rate-controlled creep-like behaviour, or at least employing great caution in using the terms plasticity and ductility in their descriptive sense.

In this discussion, it is assumed that the buoyant stresses of a diapir can simply be superimposed in a linear fashion on the strength profile of the crust deforming at a constant (depth-independent) strain rate due to regional (large-scale) tectonic movements. This linear superimposition is a simplification of reality since heterogeneous stress distribution such as that around crack tips (dikes), and non-linearity of the rheology such as non-Newtonian creep laws, will cause non-linear changes in the stress distribution. However, the assumption is still valid as a simplified mental model within one order of magnitude of accuracy, since the stress amplification around crack tips represents local heterogeneity on the scale of the crack length. As long as the magnitude of far field stresses is insufficient to cause an unstable crack growth, this local stress heterogeneity will not greatly affect large-scale stress distribution and will be balanced by surface forces, or in other words, the crack growth rate is controlled by the fact that the system lacks sufficient energy for the creation of new surfaces. Furthermore, numerous experiments with non-Newtonian (power-law) rheologies and diapiric flows lead us to the 'experimental' conclusion that changes related to non-linear rheologies mostly affect the strain rate distribution while the stress distribution remains relatively unaffected, further supporting the assumption here of linear superimposition of stresses.

If the crust is assumed to be an unbounded homogeneous visco-plastic (Bingham) material, the small buoyant stress caused by a spherical diapir alone (no tectonic stresses) is unlikely to reach the large yield strength of the crust at any depth, unless pore pressure nearly equals the lithostatic pressure (see Weinberg & Podladchikov 1994). For low pore pressure this implies that the depth of the b–d transition is close to zero. The introduction of the free upper surface (the Earth's surface) and depth dependence of the yield strength into the model do not change this conclusion, except for the extreme case of a very large and shallow pluton (Schultz-Ela *et al.* 1993). Consider now a hypothetical crust submitted to very small differential stresses. Except for a very thin upper layer of brittle behaviour, the whole crust will deform at very slow strain rates in a ductile (viscous) fashion. If the diapiric stresses can be added to such a profile by ignoring stress heterogeneities, most of the crust in this case is still likely to behave as a ductile body.

However, crustal rocks will only behave as a plastic (brittle) material when submitted to stresses high enough to equal the yield strength. In orogenic areas, high tectonic stresses will cause a thick upper crustal layer to behave in a brittle manner. In this case, the diapir may reach the b–d transition and interact with it in a complex way; the dynamics of such interactions are still not fully understood. As the brittle layer has already attained its yield strength and no further stresses can be

sustained, the addition of buoyant stresses may cause unlimited deformation of the overlying crust mainly along pre-existing faults, as evidenced by the common descriptions of crustal pluton–fault zone interaction in modern structural geological literature (e.g. the permitted intrusions of Hutton 1988). Conversely, it may be argued that if the encroaching diapir adds tensional stresses to a brittle layer under compression, the resulting differential stress will decrease below the Byerlee law and allow further ductile deformation. If the diapir is still warm, heat diffused away from it may warm up and soften the wall rocks pushing the base of the brittle layer upwards. A combination of these two mechanisms may explain the appearance of numerous shallow plutons surrounded by crust deformed in a ductile fashion, at levels where brittle behaviour is expected (e.g. Paterson *et al.* 1991).

If diapirs are to rise through cold middle to upper crust, it is necessary to look into strain-rate-dependent mechanisms (power-law rheological relationship) that allow rock flow at low temperatures and stresses below the yield stress. It is often thought that creep ceases at temperatures below half the homologous temperature (less than 50% of the melting temperature). However, a number of natural examples of fluid-like folding of rocks at 'all spatial scales' (Turcotte & Schubert 1982 p. 335) have been noted. Furthermore, rock has been seen to deform by diffusive mass transfer processes in low-grade metamorphic environments, particularly in the range of 150–350°C and confining pressure 2–8 kb (McClay 1977). Quartz, generally considered to be the weakest rock component and to control crustal deformation, shows deformation by intracrystalline plasticity under low and medium metamorphic grades, at temperatures as low as 300°C in naturally deformed rocks (Fitz Gerald & Stünitz 1993 and references therein). Experimentally deformed water-saturated Westerly granite shows complete creep curves at room temperature (Wawersick & Brown 1973, Wawersick 1974). Several authors have shown that even at room temperature porous sandstone, quartzite, basalt, marble and limestone may override the b–d transition when confining pressure is increased (see Fredrich *et al.* 1989 for references). To account for low temperature deformation there are a number of rate-dependent mechanisms that deform the rocks at stresses below the frictional yield stress, such as pressure solution creep or the equivalent Coble creep in dry rocks (McClay 1977, Turcotte & Schubert 1982 p. 335, Wheeler 1992); 'superplasticity' or viscous grain boundary sliding (Schmid *et al.* 1977, Schmid & Handy 1991); intracrystalline plasticity involving dynamic (syntectonic) subgrain rotation recrystallization or neocrystallization (Schmid & Handy 1991, Hirt & Tullis 1992, Fitz Gerald & Stünitz 1993); transformation- and reaction-enhanced ductility (White & Knipe 1978, Fitz Gerald & Stünitz 1993); creep due to hydrolytic weakening or stress corrosion of cracks (Griggs & Blacic 1965, Kirby & McCormick 1989, Scholz 1990 p. 32); and creep due to time-dependent crack growth and evolving crystal damage known as 'static fatigue' or 'brittle creep' (Scholz 1990 p. 34, Kirby & McCormick 1989, Lyakhovsky *et al.* 1993). In all these cases the general model of buoyant diapir rise in power-law fluid is still valid. In this context, it is interesting to note the commonly cited experimental observation that the effect of decreasing stress and increasing temperature on deformation mechanisms are similar (Heard 1976, Frost & Ashby 1982, Kirby & McCormick 1989 p. 189, Hirt & Tullis 1992, Wheeler 1992). Progressive temperature increase (progressive stress decrease) causes first a change from frictional to ductile (viscous) rheological behaviour and then a gradual decrease in the power-law exponent of the fluid (degree of non-linearity of creep). Additionally, Schmid & Handy (1991) argued that large strain deformation promotes frictional to viscous transition. Since diapirism is associated with small stresses and large strains, these observations must be taken into account.

In summary, although the rheology of post-orogenic and anorogenic crust may be closely approximated by that of viscous fluids, in orogenic zones the brittle–ductile transition depends on the complex interaction between stress and temperature of the crust and diapir.

## THE RISE OF A DIAPIR THROUGH A TWO-LAYERED CRUST

With the help of the computer code RISE (Appendix A), we integrated the rise of a 5-km radius diapir from the base of the crust (Figs. 3a–c), through a lower crust composed of Adirondacks granulite (rheology given by Wilks & Carter 1990), and an upper crust composed of Westerly granite (from Carter *et al.* 1981). The parameters controlling the ascent of the diapir are listed in Table 1. During the first part of the ascent, the diapir was composed of a totally liquid eutectic melt that rises and cools. At a depth of 21.7 km the diapir's temperature reached the eutectic temperature and the magma started to solidify accompanied by an increase in density. After 0.4 Ma and a 1.3 km rise, magma crystallization ends. From this point onwards two extreme cases are shown (Fig. 3a), both with $\Delta\rho = 200$ kg m$^{-3}$: (i) the rock in the diapir is inviscid as compared to the wall rock (viscosity

Table 1. Parameters controlling the ascent of a diapir through a two-layered crust. Adirondacks granulite forms the lower crust extending from 40 to 25 km, and Westerly granite forms the upper crust

| | Lower crust<br>Adirondacks granulite | Upper crust<br>Westerly granite |
|---|---|---|
| $r$ (km) | 5.0 | 5.0 |
| $H$ (km) | 40.0 | 25.0 |
| $T_{init}$ magma (°C) | 1000 | |
| $T_{sol}$, magma (°C) | 650 | 650 |
| $k$ (m$^2$ s$^{-1}$) | $10^{-6}$ | $10^{-6}$ |
| $\Delta\rho$ (kg m$^{-3}$) | 500 | 400 |
| Geothermal grad. (°C km$^{-1}$) | 25 | 25 |
| $E$ (kJ mol$^{-1}$) | 243 | 106 |
| $A$ (MPa$^{-n}$ s$^{-1}$) | $8 \times 10^{-3}$ | $1.26 \times 10^{-9}$ |
| $n$ | 3.1 | 2.9 |

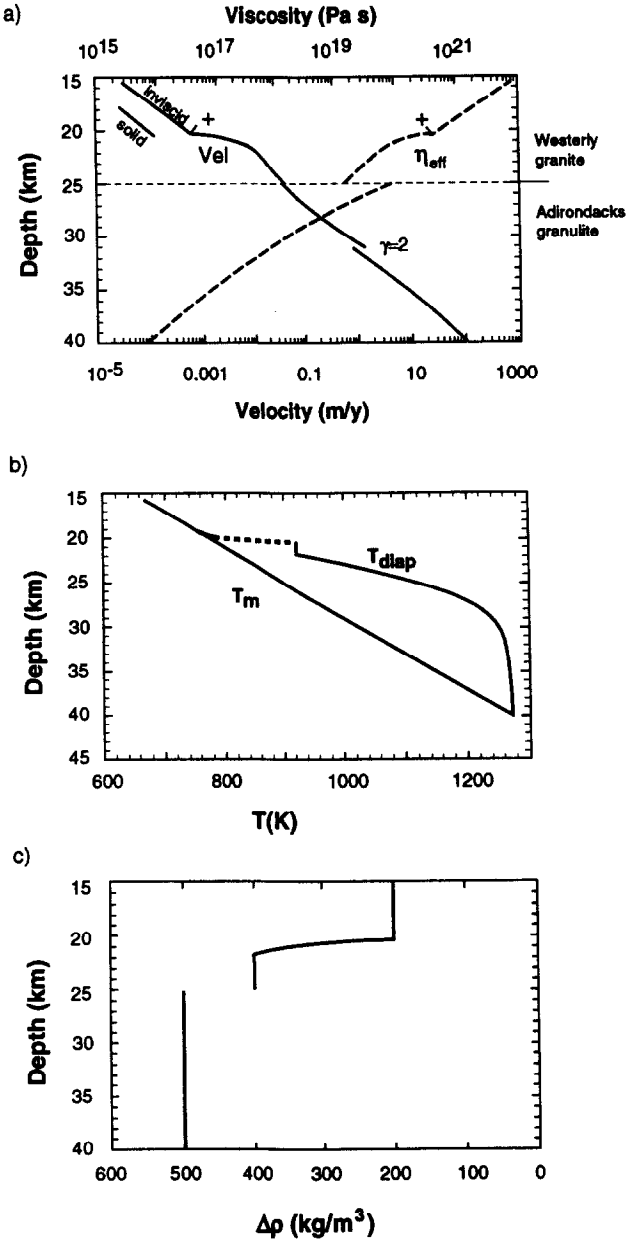


Fig. 3. The rise of a diapir through a two-layered crust (see parameters in Table 1). (a) Velocity (solid line) and effective viscosity (broken line) plotted against depth. The diapir starts at 40 km depth at a velocity of 100 m $y^{-1}$ and slows as it rises. A sharp increase in the velocity occurs when the logarithm of the ratio between the viscosities far from and close to the diapir, $\gamma = 2$, and drag reduction due to thermal softening accelerate the rise rate (see Daly & Raefsky 1985, and Weinberg & Podladchikov 1994). A smaller acceleration occurs also when the diapir leaves the stiff Adirondack granulite and enters the Westerly granite at 25 km depth. At a depth of approximately 21.5 km the diapir reaches the solidus temperature of the magma and starts to crystallize and loose buoyancy. Crystallization ends after 0.4 Ma (indicated on the figure by '+') and the density difference stabilizes at 200 kg $m^{-3}$. Two extreme cases are shown: one is a fast-rising effectively inviscid diapir and the other is effectively solid. (b) Regional temperature profile ($T_m$) and the diapir's temperature as a function of depth. (c) Density difference ($\Delta\rho$) between diapir and wall rock during ascent, as a function of depth.

ratio $S < 10^{-3}$), and (ii) the rock in the diapir is solid as compared to the wall rocks ($S > 10^3$). The inviscid diapir rose another 2.6 km in 10 Ma and 4.6 km in 50 Ma, whereas the solid diapir, rising five times slower than the inviscid diapir, rose 0.9 and 2.5 km in similar times. The slow ascent of solid mid-crustal diapirs implies that the

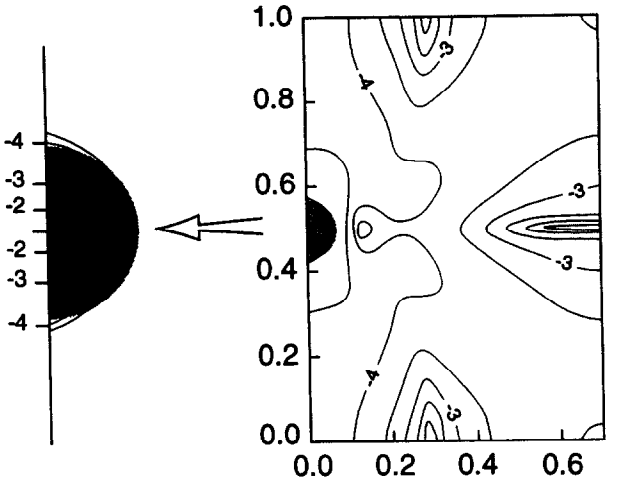


Fig. 4. Vertical section showing isoviscous lines inside and around a power-law cylinder (shaded semi-circle) of $n = 5$ rising (upward in the figure) through a power-law fluid of $n = 5$. The system is isothermal and only half the cylinder is shown, the other half is mirrored by the left-hand side boundary.

structural evolution of the diapir will be affected by other slow crustal processes such as tectonic deformation, erosion and denudation. Although the solid-state diapir rises slowly, this ascent contributes considerably to the formation of subsolidus structures observed in the field in and around plutons. Several of the distinctive structures used previously to distinguish between pre-, syn- and post-tectonic plutons become therefore questionable (see 'Discussion').

## VISCOSITY AND STRAIN RATE IN AND AROUND DIAPIRS

The general pattern of isoviscous lines around power-law diapirs of two-dimensional cylindrical shape (circular in vertical section and horizontal long axis) rising through power-law fluids at constant temperature is shown in Fig. 4. The viscosity distribution inside the rising cylinder is concentric, whereas the viscosity distribution in the ambient fluid tends to form a low viscosity channel along the direction of ascent of the cylinder. An important feature of Fig. 4 is the absence of a viscosity jump across the contact between the cylinder and the ambient fluid. As will be seen below this is not simply a result of the choice of parameters for that particular calculation, but rather a general feature of rising power-law diapirs.

A Newtonian and a power-law cylinder with the same effective viscosity contrast to the ambient fluid have different patterns of strain-rate distribution in profiles along their equator (Fig. 5). Whereas the strain rates of Newtonian cylinders and spheres increase linearly as a function of radial distance from the centre ($\dot{\varepsilon} \propto r$), those of power-law cylinders increase as a power-law function of the distance from the centre. This leads to a more homogeneous strain distribution in Newtonian cylinders than in power-law cylinders. The latter have a stiffer

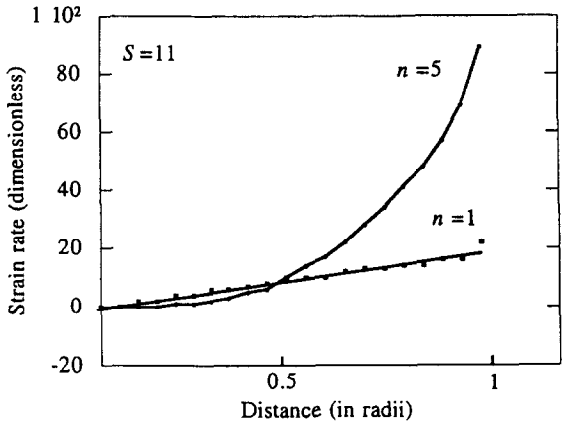


Fig. 5. Strain rate in power-law ($n$ = 5) and Newtonian ($n$ = 1) cylinders, from the centre to the contact of the cylinder along the equator. The strain rate is calculated by subtracting the dimensionless vertical velocity of two points along the horizontal profile and dividing by the dimensionless distance between them. Difference in horizontal velocities, which add to the total strain rate, could be disregarded because horizontal velocity along the cylinder equator is zero.

slow-deforming core surrounded by a softer fast-straining marginal zone where most deformation is taken up. Although the strain-rate distribution changes for the two cases above, the circular cross-section of the cylinder is retained throughout ascent. In these calculations, thermal effects are ignored, but the difference in behaviour of Newtonian and power-law cylinders would remain if these effects were also considered.

Since the strain rate for power-law fluids is proportional to the inverse of viscosity to the power of $m$-1 (where $m = 1/n$), viscosity profiles can be roughly read as the inverse of strain rate. We found that the simplest way of understanding the patterns of viscosity and strain-rate distribution in and around diapirs was to concentrate on what happens at the contact between the rising diapir and the ambient fluid. This is because the stress at the contact $\sigma_{cont}$ acts on particles that belong to both the diapir and wall rock:

$$\sigma_{cont} = \dot{\varepsilon}_{diap}\eta_{diap} = \dot{\varepsilon}_{wr}\eta_{wr}, \qquad (4)$$

where $\dot{\varepsilon}$ is the strain rate, $\eta$ the viscosity and the subscripts *diap* and *wr* denote the diapir and wall rock, respectively. For Newtonian diapirs and wall rocks the change in $\dot{\varepsilon}$ across the contact is inversely proportional to the viscosity ratio of the two fluids. In other words, a large jump in viscosity results in a large jump in strain rate.

A jump in viscosity and strain rate across the contact is also observed when a Newtonian cylinder rises through a power-law fluid (Fig. 6a). The viscosity profile of the ambient fluid along the equatorial plane is complex but varies little with changing viscosity of the interior fluid (varying $S$). The two cases shown for $S > 1$ have exactly the same pattern, whereas for $S < 1$ there is a dislocation of the viscosity maximum towards the contact. This viscosity maximum is the expression of a stagnant point in the flow cell around the rising cylinder, and its

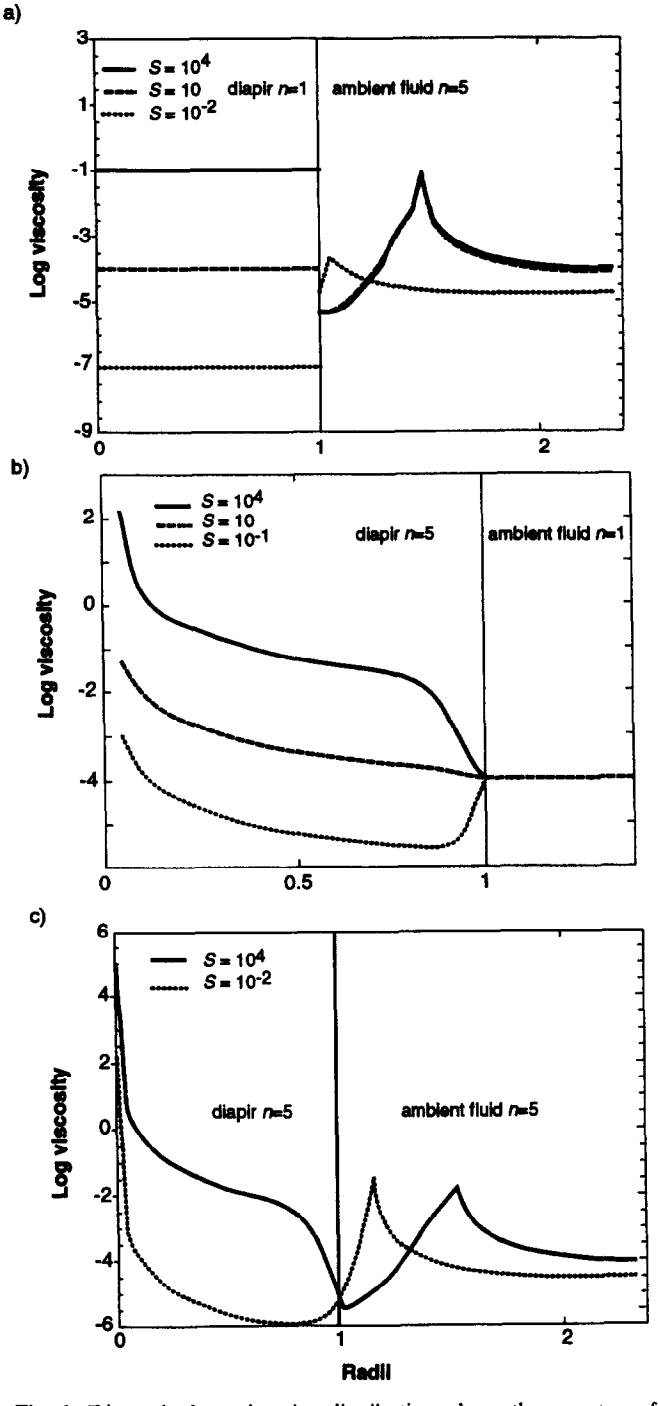


Fig. 6. Dimensionless viscosity distribution along the equator of buoyant cylinders: (a) Newtonian cylinders of three different viscosities; (b) power-law cylinders of three different values of effective viscosity contrast rising through Newtonian fluid; (c) two power-law cylinders of different effective viscosities rising through power-law fluid.

movement towards the cylinder when $S < 1$ indicates a smaller flow cell. The absolute values of the effective viscosity of the ambient fluid vary little between the different cases, indicating that the viscosity is primarily controlled by the total buoyant stress and total flow pattern imposed by the ascending cylinder, and only secondarily by the viscous drag along the contact with the cylinder. The invariable viscosity of the Newtonian cylinder and the constant stress at the contact fixes the strain rate of the cylinder, which is independent of the strain rate of the wall rock. A geologically important

feature of Fig. 6(a) is that the viscosity of the ambient fluid is lowest and the strain rate highest at the contact, regardless of the effective viscosity contrast.

This pattern changes when the rising cylinder is composed of a power-law fluid and the ambient fluid is Newtonian (Fig. 6b). The pattern for all $S$-values is very similar: the centre of the cylinder has a very high viscosity that decreases as a power-law function of the radial distance towards the contact (Fig. 6b). At a certain point the viscosity deviates from this pattern and goes towards the value of viscosity of the ambient fluid so that the viscosities on either side of the contact are the same. Figure 6(b) indicates three important features of power-law cylinders that also apply for spheres: (i) the very centre of the cylinder has zero strain rate and infinite viscosity, (ii) since the viscosities on both sides of the contact are the same, the strain rates are also the same (equation 4), indicating that the ambient fluid imposes its strain rate across the cylinder's contact, and (iii) inside the cylinder the maximum strain rate is at the contact for $S > 1$ (cylinder more viscous than the ambient fluid), and moves inwards from the contact for $S < 1$.

Comparison of Figs. 6(a) & (b) indicates that the strain rate of the external fluid controls the strain rate inside the power-law cylinder close to the contact, but that this is not the case for a Newtonian cylinder. This control leads to a smooth transition in viscosity and strain rate across the contact with the ambient fluid. Naturally this result is also valid for spheres since the principles and geometry controlling the ascent are the same. The most general case, that of power-law cylinder and ambient fluid (Fig. 6c), is a combination of the results of the last two cases. All parameters of equation (4) are free to vary for a given stress. However, Fig. 6(c) shows that all viscosity profiles pass through the same value at the contact between the cylinder and ambient fluid, this viscosity is only a function of the buoyant stress of the cylinder (the same for all cases). This results in smooth variations of viscosity and strain rate, and the solution for equation (4) at the contact is $\dot{\varepsilon}_{diap} = \dot{\varepsilon}_{wr}$ and $\eta_{diap} = \eta_{wr}$. Along the equator, the region of lowest viscosity (maximum strain rate) is just outside the cylinder when $S > 1$, and dislocates to the inner part of the contact when $S < 1$. The behaviour of the ambient fluid is basically the same for the same $S$, whether the cylinder is power-law or Newtonian (compare Figs. 6a & c), and similarly the behaviour of the cylinder's viscosity is independent of the external rheology.

Although the results presented above were found for the equator of the cylinder, the smooth transitions in viscosity along the contact of Fig. 4 indicate that the same principle applies everywhere and not only along the equator. The strain values observed in two rock volumes on each side of the contact depend on the total strain history of these two rock volumes. However, the longer these volumes travel together as the diapir rises, the more similar their strain values become. In other words, given two random rock volumes with different strain histories, the most likely way to obtain a smooth strain transition across the contact is to allow rocks on both sides to strain at the same rate.

Three of the results given above are particularly significant for diapirism of power-law fluids and differ from previous results: (1) the maximum strain rate may be just inside or just outside the diapir depending on the viscosity contrast $S$, (2) there is a much stronger outward increase in strain rate within power-law diapirs as compared to Newtonian diapirs. Whereas the core of the power-law diapir is virtually rigid, its margins will be soft and deform orders of magnitude faster than the core, and (3) there is no difference in the behaviour of the two fluids at and close to the contact, although their flow-law parameters and temperature may be different. Despite the isothermal conditions of the model, these results should also apply to a hot diapir in cold surroundings. However, as a rigid carapace forms around the cooling diapir, the region of maximum strain rate may migrate inwards towards the core of the body.

## INTERNAL CONTACTS

The same arguments given above can be used to understand the viscosity and strain distribution inside a cylinder formed by two power-law fluids of different flow-law parameters (Fig. 7), which corresponds to the rise of a diapir composed of two magmas or rocks of different composition. In Fig. 7, the flow in the most internal fluid (1) behaves as in the above discussion (Fig. 6). The more external fluid (2), however, behaves differently, and simulates the flow through a channel when it is soft (case a in Fig. 7) or a stiff layer being dragged on both sides by low viscous fluids 1 and 3 (case b). The asymmetry of the viscosity distribution in fluid 2 is, in both cases, due to different viscosities of the fluids on either side (i.e. fluids 1 and 3). The side of fluid 2 which is more intensely dragged is the side in contact with the stiffest of the two surrounding fluids 1 and 3. Of particular geological relevance is the pattern observed in curve

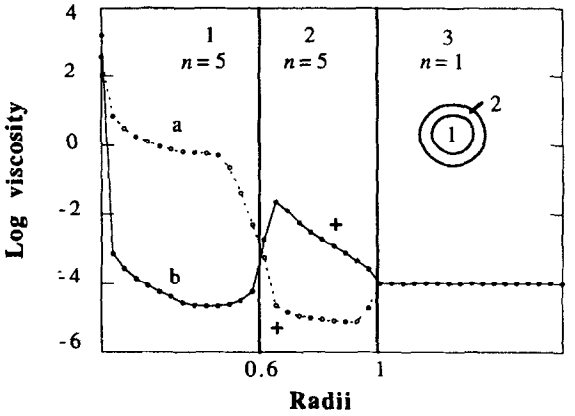


Fig. 7. Viscosity profile along the equator of two cylinders composed of two power-law ($n = 5$) fluids (1 and 2) of different scaling viscosity. The external fluid (3) is Newtonian and has a viscosity of $10^{-4}$. The two curves a and b differ in the viscosities of fluids 1 and 2. Curve a has a stiff fluid 1 and soft fluid 2, whereas curve b is the inverse. The '+' marks the side of the curve in fluid 2 which is more intensely dragged by the neighbouring fluids 1 and 3.

b where, although the stress increases outwards, the strain rate (approximately the inverse of the viscosity) in fluid 1 may be higher than that of the stiffer and more external fluid 2.

## RIM SYNFORMS

The downward flow of ambient power-law fluid around a rising cylinder causes folding of a horizontal passive marker around a diapir into a synform (Fig. 8). In non-expanding cylinders the position of the hinge of the synform can be approximated by the position of maximum downwards velocity along the equatorial plane of the cylinder (Fig. 2). For a solid sphere rising in infinite (unbounded) fluid, the synform becomes tighter and closer to the contact as $n$ increases. Figure 9 shows that the solution for a cylinder differs from that of a sphere only in that, for a cylinder, the position of the hinge is further away from the contact. This is an expected difference since a cylinder displaces a larger volume of fluid than a sphere of the same radius (see Weijermars 1988). Figure 9 suggests that velocity profiles around cylinders and spheres react similarly to changes in the values of $n$ and $S$.

If $n$ is kept constant and $S$ increased (increasing the viscosity of the cylinder), the increase in size of the flow cell causes the amplitude of the synform to decrease and the position of the hinge to move away from the contact (Fig. 10). Similar changes occur when $n$ decreases (Fig. 2). Crochet *et al.* (1984) found that for solid spheres ($S \gg 1$) synforms would form for $n > 1.7$. In contrast, no synforms were found here for cylinders of $S \geqslant 1$ rising in fluids of $n \leqslant 3$. The reason for this

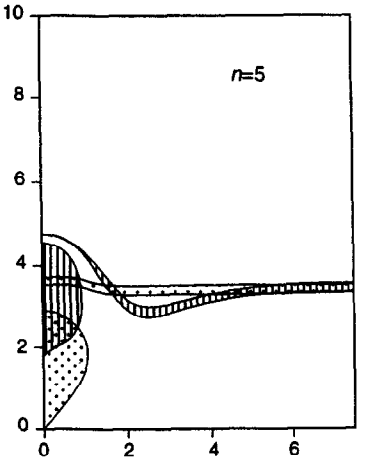


Fig. 8. Two steps during the rise of a cylinder and the folding of a passive layer of $n = 5$ into a synform. The cylinder (only half the cylinder is shown) and the passive layer are marked at each step with different patterns (in the earlier step the diapir and layer are dotted, and in a later step they have vertical lines). As the diapir rises, the passive layer folds into a synform. The position of the hinge varies only slightly as the cylinder rises, first expanding outwards and later contracting as the cylinder approaches and rises past it. The axes are dimensionless distance measured in diapir radii.

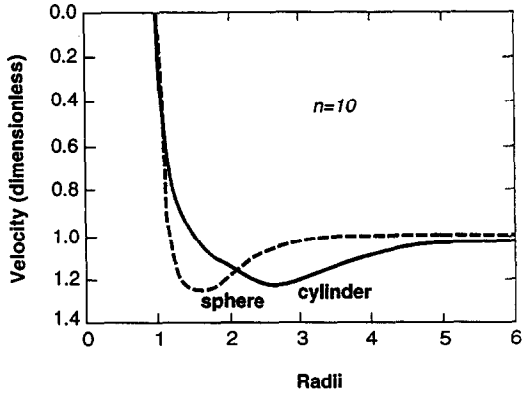


Fig. 9. Comparison between the velocity of an ambient fluid of $n = 10$, surrounding a rising cylinder and a sphere at the equatorial plane. The profile for the cylinder (solid line) was found numerically in a box 14 times wider than the cylinder radius, and that of the sphere (broken line) is from the work of Crochet *et al.* (1984) in an infinite fluid. The flow cell in the ambient fluid around the cylinder is wider, due to larger volumes displaced, causing the hinge of the velocity synform to be further away from the cylinder. The qualitative similarity between the two curves indicates that the flow around cylinders is qualitatively similar to that around spheres. The high $n$ in this figure was chosen because it enhances the velocity synform.

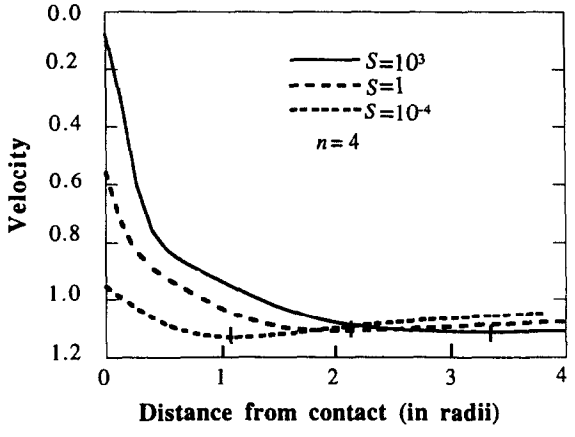


Fig. 10. Velocity profile around cylinders of increasing viscosity, for ambient fluid of $n = 4$. For low viscosity cylinders, the whole flow cell in the ambient fluid approaches the cylinder, because part of the flow is taken by the cylinder itself, and the synform hinges are closer to the contact cylinder/ambient fluid (marked with a short vertical line on the figure).

difference may be either the cylindrical geometry or the influence of the box boundaries.

The influence of lateral expansion of the diapir on the position of the hinge was studied by allowing the geothermal gradient as well as the strain-rate distribution to control the viscosity of the ambient fluid. The geothermal gradient and upward increase in viscosity cause the diapir to expand laterally and shorten vertically (see models in Kukowski & Neugebauer 1990). The rheology of the ambient fluid was that of the Westerly granite (from Carter *et al.* 1981) but instead of using $n = 2$, we chose $n = 5$ in order to increase the downward flow and increase the amplitude of the fold. Except for an increased $n$, the model ambient fluid closely corresponds to the expected behaviour of the crust inasmuch as it assumes both temperature- and stress-dependent behaviour. As the diapir rises and expands laterally, the

point of maximum downward velocity of the ambient fluid moves outwards, keeping the same distance to the contact. The hinge, however, being a result of finite strain, expands more slowly and moves closer to the contact at every step. The distance between the hinge and cylinder/ambient fluid contact remains constant for the constant temperature case, while the cylinder rises a distance of $0.6r$ through the passive marker. Allowing lateral expansion, a cylinder rising the same distance, causes the distance to the hinge to shorten from 1.8 to $1.7r$. This is due to a 10% increase in the horizontal radius of the cylinder followed by a smaller, approximately 2%, lateral expansion of the hinge. Faster lateral expansion and slow ascent velocities, such as in the late emplacement stages of a diapir, may lead to a considerable shortening of the distance to the synform hinge formed earlier in the rise of the diapir when it was rising fast.

## DISCUSSION

### *Rim synforms*

The distance of the synform hinge from the diapir's contact increases with increasing diapir viscosity and decreasing $n$-value. However, if the diapir expands laterally as it rises, this distance decreases. Comparison of velocity profiles for spheres and cylinders (Fig. 9) indicates that rim synforms are narrower around the former than around the latter. The Northern Arran granite in northwest Scotland can be used as an example. On the geological map, a rim synform (the Catacol synform) surrounds the pluton (England 1992). Based on the relation between cordierite porphyroblasts and cleavage, England (1992) demonstrated that the synform was formed during emplacement of the granite. The distance between the hinge of the synform and the contact is approximately $0.35$–$0.40\,r$. If no lateral expansion of the granite occurred, such a short distance could only be the result of the emplacement of a low viscosity spherical pluton in rocks of high $n$-value. However, if the granite also expanded laterally as it rose, such a short distance to the hinge could result from a wider range of $S$- and $n$-values. In order to further constrain the parameters that controlled the emplacement of the Northern Arran granite, it would be necessary to extend the results of Crochet *et al.* (1984) to low viscosity spheres. The rare occurrence of rim synform descriptions in the literature may indicate either a low power-law exponent of the wall rocks or simultaneous deformation by other mechanisms, as suggested by Paterson & Fowler (1993).

### *Strain in diapirs*

Strain distribution in the wall rocks of diapirs has recently been discussed by Paterson & Fowler (1993 and reply 1994) and Weinberg (1994), and we will therefore concentrate on the strain inside diapirs. Many plutonic rocks show an isotropic core and an increase in strain towards the pluton's margin, with occasional evidence of superimposition of solid-state deformation on magmatic foliation. The increase in strain towards the pluton's margins and the continuous passage from magmatic to solid-state deformation have been suggested to result from ballooning (Courrioux 1987, Ramsay 1989), from deformation of plutons as they crystallize by tectonic shortening (Castro 1987), from granitoids that intruded active shear zones (e.g. Guineberteau *et al.* 1987), or simply from the ascent of a diapir with a solid external carapace (Cruden 1990). Here we suggest that if the interior of the diapir is homogeneous and deforms by power-law creep, whether magma or rock, the strain-rate distribution is such that the core may remain weakly deformed and strain increase towards the margins, which may become highly sheared during ascent (Fig. 5).

The simultaneous effects of strain-rate softening and cooling of the diapir's margins were not studied here. On the one hand, high concentration of strain to the margins will be further enhanced by the longer strain memory of the margins, since magmas here crystallize earlier and start recording strain earlier than the pluton's interior. On the other hand, the crystallization of magmas may cause strain-rate hardening and movement of the high-strain-rate region towards the interior of the body. The final strain distribution will depend on how these two processes interact.

Although the uniaxial oblate strains observed by Ramsay (1989) in the Chindamora batholith were used as evidence for ballooning, the same strain ellipsoids could be formed by another process. The upward cooling and increase in viscosity of the crust, causes lateral expansion associated with vertical shortening of a rising diapir (i.e. a single magma batch). The higher in the crust, the sharper the upward increase in viscosity becomes and the slower the diapir rises. This leads to a continuous increase in importance of lateral spreading as compared to vertical ascent. Depending on the relative importance of expansion and rise during straining of the diapir, the strain ellipses will vary in shape from plane strain to oblate. In this way, both the Ljugaren pluton in central Sweden, with plane strains grading into general flattening strains towards the margins (Cruden & Aaro 1992), and the Chindamora batholith, would have the same emplacement mechanism but the vertical component of movement would be more important in the former than in the latter.

### *Internal contacts and ballooning*

The most common pattern of strain distribution inside plutons is that of an increase in intensity towards the margins. The Criffel pluton (Courrioux 1987) and perhaps the Chindamora batholith (Ramsay 1989) seem to be an exception to the rule. The maximum strain in the Criffel pluton is not at the margins, but close to the 2 km-wide contact between the external granodiorite and the central granite. Although ballooning, according to Courrioux (1987), satisfactorily explains the strain pat-

Table 2. A revised summary of the characteristics of pre-, syn- and post-tectonic plutons (based on Paterson 1988, and Paterson & Tobisch 1988). Some of the characteristics that were previously thought to belong to diapirs of a particular relative age in relation to tectonic deformation, are listed as characteristics that can be found in diapirs of all ages. As noted by Paterson & Tobisch (1988) no single criterion is sufficient to establish the relative timing between emplacement and regional deformation

| All diapirs |
|---|
| 1. Emplacement-related ductile shear zones along the pluton's margins. |
| 2. May or may not appear deformed. |
| 3. Contacts apparently cutting the structures in the wall rock. |
| 4. Aureole porphyroblasts with varying timing relationships. |
| 5. Concordance of magmatic and/or solid-state foliation with the pluton's boundaries. |
| 6. Gradation between regional and pluton strains (increase in deformation intensity inside the pluton towards the contact, and decrease in intensity in the country rocks away from the contact). |
| 7. Continuity of stretching lineation. |

| Pre-tectonic | Syn-tectonic | Post-tectonic |
|---|---|---|
| 1. Regional ductile shear zones. | 1. Cleavage triple points. | 1. Magmatic foliation inside the pluton and decreasing inwards. |
| 2. Strain shadows for high viscosity plutons ($S > 1$). | 2. Synkinematic metamorphic assemblage, highest grade near the pluton. | 2. Penetrative foliation in the country rock, within a few kilometres of the contact, centred on the diapir. |
| 3. Pluton deformed throughout for low viscosity plutons ($S < 1$). | 3. Pluton deformed throughout. | 3. Syn-emplacement metamorphic assemblage, highest grade near the pluton. |
| 4. Thermal aureole overprinted by younger tectonic foliation related to regional strain. | 4. Concordance of pluton shape with regional structure. | |
| 5. Orientation of solid-state foliation in the pluton independent of pluton boundaries. | | |

terns observed in this pluton, this work proposes a simple alternative. Curve b in Fig. 7 indicates that if two magmas or rocks in a rising diapir have different flow-law parameters, a zone of high strain rate (low viscosity) may develop close to their contact, without the need for ballooning.

How to distinguish between a magma batch being ballooned by a younger pulse of magma and a more simple case of simultaneous rise of two magmas or rocks of different rheologies? Both models would cause the superposition of solid-state foliation on any previously formed magmatic foliation, but only ballooning would have a strong discontinuity in strain across the internal contact. This discontinuity develops because in the ballooning model the two magma batches have different strain and cooling histories (Courrioux 1987, Ramsay 1989), whereas in the case of simultaneous rise of two magmas or rocks their history is the same and there are no jumps in temperature or strain rate across the contact.

*Relative age of tectonic deformation and plutons*

It is essential to understand the structures formed during diapiric emplacement of magmas in order to decipher the relative age of emplacement and tectonic deformation. The rapid cooling and slow ascent during the last stages of crystallization of the magma (Fig. 3b) and even thereafter, may cause difficulties in assessing the relative ages of pluton emplacement and regional metamorphism and deformation. The features characteristic of different relative emplacement ages summarized by Paterson (1988) and Paterson & Tobisch (1988) considered that diapirs stop rising when solidification is advanced. Table 2 revises such features assuming that solid-state diapirs are able to rise.

It is clear from the above results that even a post-tectonic diapir can create, during emplacement, a cold solid-state concentric foliation inside and outside its contacts, without the help of ballooning. This late foliation, regardless of whether or not it is associated with retrogressive mineral assemblages, may overprint early high-temperature porphyroblasts grown in the metamorphic aureole of a diapir. The suggestion that low to moderate temperature mineral assemblage defining a foliation inside the pluton might indicate a tectonic origin for the foliation does not seem to hold in all cases.

The differences in the internal deformation of approximately contemporaneous syn-tectonic augen gneiss domes and plutonic domes in the Pyrenees may be due to viscosity differences in the rising diapirs (Soula 1982). The plutonic domes described by Soula (1982), that present magmatic foliations slowly progressing outwards to a mylonitic foliation, may have become an almost rigid object upon solidification and their interior became protected from further deformations. The gneiss domes, on the other hand, may have had low viscosity during and after emplacement and were deformed throughout by their rise and by syn-emplacement regional deformation (see viscosity profiles in Figs. 6b & c). In contrast to the interpretation of Soula (1982), we believe that mushroom-shaped or inverted pear-shaped diapirs are not necessarily the result of diapirs of similar viscosity to the wall rock. Low-viscosity diapirs will, as discussed above, become flattened and mushroom-shaped as they rise through the crust, due to the upward increase in viscosity.

The above reasoning helps understanding of the behaviour of pre-tectonic plutons, regardless of their intrusion mechanisms. Whether or not a pluton deforms during later tectonic events depends mainly on the effective viscosity contrast between pluton and wall-

rock. During tectonic deformation a low viscosity pluton ($S < 1$) will deform throughout, whereas deformation of a stiff pluton ($S > 1$) is restricted to its margins. Paterson *et al.* (1989) described pre-tectonic plutons in west-central Sierra Nevada, where an older hornblende diorite with virtually no quartz or mica lacks a foliation and is only weakly recrystallized, whereas a younger pluton rich in quartz and mica has a well developed solid-state foliation continuous with wall-rock foliation. Paterson & Tobisch (1988) described the Guadalupe Igneous Complex in terms of undeformed igneous rocks except for several hundred metres close to the contact with the wall rock on the western margin, where post-emplacement deformation is concentrated. The deformation pattern in this complex may be interpreted based on our results for high $S$-values, with concentration of deformation along the contact between wall rock and pluton where tectonic drag causes the contact region of the pluton to deform at the same rate as the wall rock, and a rapid decrease in strain rate inwards. The width of the strained area inside the pluton depends on the viscosity contrast, strain rate and duration of the regional deformation.

## CONCLUSION

The study of strain rate and viscosity distribution in and around a power-law diapir, whether composed of mush or crystalline rock, suggests that such diapirs rise with a high effective viscosity, low strain rate core surrounded by a low effective viscosity, high strain rate margin where most of the deformation is accommodated. This accounts for the commonly observed increase in strain intensity from the diapir's centre to its borders. The strain rate of the external fluid is able to impose a similar strain rate across the contact with the rising fluid, leading to a smooth strain gradation across the contact. The region of maximum strain rate is just outside or just inside the diapir depending on whether the diapir has, respectively, high or low effective viscosity. As the diapir rises, and if the power-law exponent is sufficiently high, the ambient fluids may fold into a synform. The presence and shape of such rim synforms may help in constraining the wall rock's rheology and the viscosity contrast to the intruding pluton.

If a magmatic diapir is still lighter than its surroundings after magma crystallization, the diapir does not stop rising but may continue to rise a few kilometres in the solid state. This rise provides alternative explanations for a series of commonly observed features in and around diapirs and causes complication in the interpretation of the relative age of emplacement and tectonic deformation. For example, the solid-state rise of diapirs may cause the superposition of a solid-state foliation on a magmatic foliation inside the diapir and of a low-grade late foliation on an early high-grade mineral assemblage of the metamorphic aureole. If the diapir is composed of two or more magmas or rocks of different rheologies, a high strain region may form inside the diapir close to the contact between the two when the magma or softer rock is interior to the stiffer one.

*Acknowledgements*—We would like to thank Prof. Christopher Talbot for his support of the present work and Prof. Harro Schmeling for the use of his computer code and computer facilities. We are also grateful to Dr Ross Kerr for commenting an early version of the manuscript, and Drs Nina Kukowski and Scott Paterson for detailed and constructive review of the manuscript. Thanks also to Christina Wernström for drawing the figures and Sharon Ford for language editing.

## REFERENCES

Arndt, N. T. & Goldstein, S. L. 1989. An open boundary between lower continental crust and mantle: its role in crust formation and crustal recycling. *Tectonophysics* **161**, 201–212.

Carter, N. L., Anderson, D. A., Hansen, F. D. & Kranz, R. L. 1981. Creep and creep rupture of granitic rocks. *Geophys. Monograph, Am. Geophys. Union* **24**, 61–82.

Carter, N. L. & Tsenn, M. C. 1987. Flow properties of continental lithosphere. *Tectonophysics* **136**, 27–63.

Castro, A. 1987. On granitoid emplacement and related structures. A review. *Geol. Rdsch.* **76**, 101–124.

Courrioux, G. 1987. Oblique diapirism: the Criffel granodiorite/granite zoned pluton (southwest Scotland). *J. Struct. Geol.* **9**, 313–330.

Crochet, M. J., Davies, A. R. & Walters, K. 1984. *Numerical Simulation of Non-Newtonian Flow*. Rheology Series, Elsevier, New York.

Cruden, A. R. 1988. Deformation around a rising diapir modelled by creeping flow past a sphere. *Tectonics* **7**, 1091–1101.

Cruden, A. R. 1990. Flow and fabric development during the diapiric rise of magma. *J. Geol.* **98**, 681–698.

Cruden, A. R. & Aaro, S. 1992. The Ljugaren granite massif, Dalarna, central Sweden. *Geol. För. Förh.* **114**, 209–225.

Daly, S. F. & Raefsky, A. 1985. On the penetration of a hot diapir through a strongly temperature-dependent viscosity medium. *Geophys. J. R. astr. Soc.* **83**, 657–681.

England, P. 1992. The genesis, ascent, and emplacement of the Northern Arran Granite, Scotland: Implications for granitic diapirism. *Bull. geol. Soc. Am.* **104**, 606–614.

Fitz Gerald, J. D. & Stünitz, H. 1993. Deformation of granitoids at low metamorphic grade. I: Reactions and grain size reduction. *Tectonophysics* **221**, 269–297.

Fredrich, J. T., Evans, B. & Wong, T. F. 1989. Micromechanics of the brittle to plastic transition in Carrara Marble. *J. geophys. Res.* **94**, 4129–4125.

Frost, H. J. & Ashby, M. F. 1982. *Deformation mechanisms maps: the plasticity and creep of metals and ceramics*. Pergamon, Oxford.

Glazner, A. F. 1994. Foundering of mafic plutons and density stratification of continental crust. *Geology* **22**, 435–438.

Griggs, D. T. & Blacic, J. D. 1965. Quartz-anomalous weakness of synthetic crystals. *Science* **147**, 292–295.

Guineberteau, B., Bouchez, J.-L. & Vigneresse, J. L. 1987. The Mortagne granite pluton (France) emplaced by pull-apart along a shear zone: structural and gravimetric arguments and regional implications. *Bull. geol. Soc. Am.* **99**, 763–770.

Hadamard, J. 1911. Mouvement permanent lent d'une sphere liquide et visqueuse dans un liquid visqueux. *C. r. Acad. Sci.* **152**, 1735–1738.

Heard, H. C. 1976. Comparison of the flow properties of rocks and minerals: strength and rheology. *Phils. Trans. R. Soc. Lond.* **A283**, 173.

Hirt, G. & Tullis, J. 1992. Dislocation creep regimes in quartz aggregates. *J. Struct. Geol.* **14**, 145–159.

Hutton, D. H. 1988. Granite emplacement mechanisms and tectonic controls: inferences from deformation studies. *Trans. R. Soc. Edinb.* **79**, 245–255.

Kerr, R. C. & Lister, J. R. 1991. The effects of shape on crystal settling and on the rheology of magmas. *J. Geol.* **99**, 457–467.

Kirby, S. H. 1983. Rheology of the lithosphere. *Rev. Geophys. & Space Phys.* **21**, 1458–1487.

Kirby, S. H. & McCormick, J. W. 1989. Inelastic properties of rocks and minerals: strength and rheology. In: *Practical Handbook of Physical Properties of Rocks and Minerals* (edited by Carmichael, R. S.). CRC Press, Inc.

Kukowski, H. & Neugebauer, H. J. 1990. On the ascent and emplacement of granitoid magma bodies. Dynamic-thermal numerical models. *Geol. Rdsch.* **79**, 227–239.
Lyakhovsky, V., Podladchikov, Yu., & Poliakov, A. 1993. Rheological model of a fractured solid. *Tectonophysics* **226**, 187–198.
Mahon, K. I., Harrison, T. M. & Drew, D. A. 1988. Ascent of a granitoid diapir in a temperature varying medium. *J. geophys. Res.* **93**, 1174–1188.
Mandl, G. 1988. *Mechanics of Tectonic Faulting*. Elsevier, Amsterdam.
Marsh, B. D. 1982. On the mechanics of igneous diapirism, stoping, and zone melting. *Am. J. Sci.* **282**, 808–855.
McClay, K. R. 1977. Pressure solution and Coble creep in rocks and minerals: a review. *J. geol. Soc. Lond.* **134**, 57–70.
Miller, C. F., Watson, M. E. & Harrison, T. M. 1988. Perspective on the source, segregation and transport of granitoid magmas. *Trans. R. Soc. Edinburgh* **79**, 135–156.
Nakano, Y. & Tien, C. 1968. Creeping flow of power-law fluid over Newtonian fluid sphere. *A. I. Ch. E. Jl.* **14**, 145–151.
Ord, A. & Hobbs, B. E. 1989. The strength of the continental crust, detachment zones and the development of plastic instabilities. *Tectonophysics* **158**, 269–289.
Paterson, M. S. 1987. Problems in the extrapolation of laboratory rheological data. *Tectonophysics* **133**, 33–43.
Paterson, S. R. 1988. Cannibal Creek granite: post-tectonic "baloon-ing" pluton or pre-tectonic piercement diapir? *J. Geol.* **96**, 730–736.
Paterson, S. R. & Fowler, T. K., Jr. 1993. Re-examining pluton emplacement processes. *J. Struct. Geol.* **15**, 191–206.
Paterson, S. R. & Fowler, T. K., Jr. 1994. Re-examining pluton emplacement processes: reply. *J. Struct. Geol.* **16**, 747.
Paterson, S. R. & Tobisch, O. T. 1988. Using pluton ages to date regional deformation: problems with commonly used criteria. *Geology* **16**, 1108–1111.
Paterson, S. R., Vernon, R. H. & Fowler, T. K. 1991. Aureole tectonics. In: *Reviews in Mineralogy* (edited by Kerrick, D. M.). Book Crafters, 673–722.
Paterson, S. R., Vernon, R. H. & Tobisch, O. T. 1989. A review of criteria for the identification of magmatic and tectonic foliations in granitoids. *J. Struct. Geol.* **11**, 349–363.
Pinkerton, H. & Stevenson, R. J. Submitted. Methods of determining the rheological properties of magmas at sub-liquidus temperature. *J. Volcanol. & Geotherm. Res.* **53**, 47–66.
Ramsay, J. G. 1989. Emplacement kinematics of a granite diapir: the Chindamora batholith, Zimbabwe. *J. Struct. Geol.* **11**, 191–209.
Rutter, E. H. 1986. On the nomenclature of mode of failure transitions in rocks. *Tectonophysics* **122**, 381–387.
Rybczynski, W. 1911. Über die fortschreitende Bewegung einer flüssigen Kugel in einen zähen Medium. *Bull. Acad. Sci. Cracovie* **1**, 40–46.
Schmeling, H., Cruden, A. R. & Marquart, G. 1988. Finite deformation in and around a fluid sphere moving through a viscous medium: implications for diapiric ascent. *Tectonophysics* **149**, 17–34.
Schmid, S. M., Boland, J. N. & Paterson, M. S. 1977. Superplastic flow in finegrained limestone. *Tectonophysics* **43**, 257–291.
Schmid, S. M. & Handy, M. R. 1991. Towards a genetic classification of fault rocks: geological usage and tectonophysical implications. In: *Controversies in Modern Geology, Evolution of Geological Theories in Sedimentology, Earth History and Tectonics* (edited by Muller, D. W., McKenzie, J. A. & Weissert, H.). Academic Press, London, 339–361.
Scholz, C. H. 1990. *The Mechanics of Earthquakes and Faulting*. Cambridge University Press, Cambridge.
Schultz-Ela, D. D., Jackson, M. P. A. & Vendeville, B. C. 1993. Mechanics of active salt diapirism. *Tectonophysics* **228**, 275–312.
Shaw, H. R. 1969. Rheology of basalt in the melting range. *J. Petrol.* **10**, 510–535.
Soula, J. C. 1982. Characteristics and mode of emplacement of gneiss domes and plutonic domes in central-eastern Pyrenees. *J. Struct. Geol.* **4**, 313–342.
Spera, F. J., Borgia, A. & Strimple, J. 1988. Rheology of melts and magmatic suspensions 1. Design and calibration of concentric viscometer with application to rhyolitic magma. *J. geophys. Res.* **93**, 10,273–10,294.
Turcotte, D. L. & Schubert, G. 1982. *Geodynamics: Application of Continuum Physics to Geological Problems*. Wiley, New York.
Vigneresse, J. L. 1988. Forme et volume des plutons granitiques. *Bull. geol. Soc. Fr.* **8**, 897–906.
Wawersick, W. R. 1974. Time-dependent behavior of rock compression. In: *Advances of Rock Mechanics*. Proc. 3rd Congress Int. Soc. Rock Mech. Vol. 2 (Part A), National Academy of Science, Washington D.C.
Wawersick, W. R. & Brown, W. S. 1973. Creep fracture of rocks. Advance Research Projects Agency, Order No. 1579, Program Code 2F10, Department of Defence, Washington D.C.
Weijermars, R. 1988. New laboratory method for analyzing deformation and displacement in creeping fluid: examples from Stokes flow and a thermal plume. *J. geophys. Res.* **93**, 2179–2190.
Weinberg, R. F. 1992. Internal circulation in a buoyant two-fluid Newtonian sphere: implications for composed magmatic diapirs. *Earth Planet. Sci. Let.* **110**, 77–94.
Weinberg, R. F. 1994. Re-examining pluton emplacement processes: discussion. *J. Struct. Geol.* **16**, 743–746.
Weinberg, R. F. & Podladchikov, Y. 1994. Diapiric ascent of magmas through power-law crust and mantle. *J. geophys. Res.* **99**, 9543–9559.
Weinberg, R. F. & Podladchikov, Y. 1993. The low Reynolds number rise of a viscous cylinder through bounded power-law fluids. Phd.D. Thesis, Uppsala University, Uppsala, Sweden.
Weinberg, R. F. & Schmeling, H. 1992. Polydiapirs: Multiwavelength gravity structures. *J. Struct. Geol.* **14**, 425–436.
Wheeler, J. 1992. Importance of pressure solution and Coble creep in the deformation of polymineralic rocks. *J. geophys. Res.* **97**, 4579–4586.
White, S. H. & Knipe, R. J. 1978. Transformation- and reaction-enhanced ductility in rocks. *J. geol. Soc.* **135**, 513–516.
Wilks, K. R. & Carter, N. L. 1990. Rheology of some continental lower crustal rocks. *Tectonophysics* **182**, 57–77.

## APPENDIX A

*The computer code and assumptions in the calculations*

In this paper the program RISE described in Weinberg & Podladchikov (1994) is further developed in order to calculate the rise of power-law diapirs that simulate the rise of magma mushes or solid rocks. The program reads six dimensionless parameters that define the initial temperature and depth of the diapir, and the flow-law parameters of the wall rock and diapir fluid, geothermal gradient of the crust and thermal diffusivity. These parameters control the ascent velocity and cooling of the diapir. The magma is assumed to be eutectic and when it reaches the eutectic temperature, $T_{sol}$, it starts to solidify at constant temperature. During crystallization the density increases linearly, until it reaches a pre-established density upon total crystallization. The increase in density is controlled by the release of latent heat of the magma. The program calculates the total latent heat of the magma body ($H_{lat} = L\rho_{diap}V$ where $L$ is the latent heat, $\rho$ the magma density and $V$ its volume). Then it uses the heat flow out of the diapir, calculated on the last step before the magma reaches $T_{sol}$, to calculate the amount of heat consumed to maintain $T_{diap} = T_{sol}$ during following steps. When the consumed heat equals $H_{lat}$, crystallization is finished and the effective viscosity of the igneous rock is calculated according to equations (2) and (3).

Weinberg & Podladchikov (1993) determined the full equations that describe the rise of power-law cylinders. For power-law spheres the full solution remains unknown. However, for the extreme cases of solid or inviscid spheres, the solution for Newtonian spheres applies. For spherical diapirs, the program calculates the viscosity contrast $S$ using equations (2) and (3) and then, if $S \leq 1$, the program assumes the diapir to be inviscid, otherwise to be solid. This approach leads to a maximum error on the estimation of velocity of spherical diapirs of $X_{sol}M/2$ (from equation 1; for large $n = 5$ this error is approximately 5).

The assumptions involved in the calculations are:

(a) Natural diapirs rise through a geothermal gradient and the diapir radius is often sufficiently large to be in contact with rocks initially at different temperatures. This asymmetry in the temperature distribution around the diapir will influence the rise velocity, the shape and the heat loss of different parts of the diapir. However, the calculations of velocity and temperature here assume for simplicity that the diapir is much smaller than the crustal temperature gradient. In this way, the diapir is, at each step, in contact with a fluid of constant temperature. The diapir then rises to the next calculation step and a new regional temperature is calculated, controlled by the new depth. This simplification does not considerably change the results while the diapir is in the deep crust, but becomes increasingly more important as

the diapir rises to shallower crustal levels and crustal viscosity gradient becomes more sensitive to the geothermal gradient.

(b) The velocities are calculated using correction factors for spheres rising in an effectively infinite fluid. However, as the diapir rises to upper crustal levels, and the upward viscosity increase becomes sharper, the crust above the diapir acts as a no-slip top boundary to the rising diapir. Weinberg & Podladchikov (1993) showed that the presence of a boundary may either accelerate or decelerate the diapiric rise, depending on the distance between the diapir and the boundary.

(c) The temperature inside the diapir is assumed to be homogeneous at all times. If the diapir has a heterogeneous temperature distribution, the main effect will be slower cooling and therefore a narrower thermal aureole around the diapir, which in turn affects the ascent velocity of the diapir by affecting the heat softening of the wall rock. Temperature gradients inside the diapir will have no direct influence on its velocity as long as the diapir's viscosity is much less than that of the country rocks. Since the melt is of eutectic composition, the latent heat can be included and simplifies the increase in magma density calculations.

## APPENDIX B

*Two-dimensional finite difference computer code*

A two-dimensional finite difference computer code developed by Schmeling was used to study the viscosity, strain rate and velocity profiles in and around a diapir. The following equations were used in these numerical simulations

$$\frac{\partial v_i}{\partial x_i} = 0 \tag{B1}$$

$$\frac{\partial \rho}{\partial t} + v_i \frac{\partial \rho}{\partial x_i} = 0 \tag{B2}$$

$$-\frac{\partial P}{\partial x_i} + \frac{\partial \tau_{ij}}{\partial x_i} + \rho g_i = 0 \tag{B3}$$

where $v_i$ is the component of the velocity vector, $P$ the pressure, $\tau_{ij}$ the deviatoric stress tensor, $\rho$ the density, $g_i$ the component of the gravity acceleration vector, and $t$ the time. The rheological law used was

$$\tau_{ij} = K \gamma^{n-1} \dot{\varepsilon}_{ij} \quad \text{where} \quad \dot{\varepsilon}_{ij} = \frac{1}{2}\left(\frac{\partial v_i}{\partial x_j} + \frac{\partial v_j}{\partial x_i}\right) \tag{B4}$$

where $\gamma$ is the second invariant of the strain rate tensor $\dot{\varepsilon}_{ij}$

$$\gamma = \sqrt{\frac{1}{2}\left(\sum_{i,j} \varepsilon_{i,j}\varepsilon_{i,j}\right)}. \tag{B5}$$

Further details of the mathematical formulation and numerical finite difference schemes for equations (B1)–(B3) in the case of Newtonian variable viscosity are described in Weinberg & Schmeling (1992). Picard iteration was used to treat the non-linear equation (B4). The program gives the viscosity and velocity at each grid point, that are an average of the values of the markers within half a grid distance from the grid point. The boundaries were all free-slip and reflective. Due to resolution limitations, the size of the diapirs could not be made small enough to avoid small effects of the boundaries of the calculation box.